

# Onset of pulsatile waves in the heart walls at end-systole

Hiroshi Kanai <sup>a,\*</sup>, Sachiko Yonechi <sup>a</sup>, Ikuko Susukida <sup>a</sup>, Yoshiro Koiwa <sup>b</sup>,  
Hide-ichi Kamada <sup>b</sup>, Motonao Tanaka <sup>c</sup>

<sup>a</sup> Department of Electrical Engineering, Graduate School of Engineering, Tohoku University, Sendai 980-8579, Japan

<sup>b</sup> First Department of Internal Medicine, Tohoku University School of Medicine, Seiryu-machi, Aoba-ku, Sendai 980-8574, Japan

<sup>c</sup> Tohoku Welfare Pension Hospital, Takasago 10, Fukumuro, Miyagino-ku, Sendai 983-8512, Japan

## Abstract

We have previously developed a novel ultrasonic method, namely, the phased tracking method, for accurately tracking the movement of the heart wall based on both the phase and magnitude of the demodulated signals to determine the instantaneous position of an object. With this method, it is possible to accurately detect small-amplitude velocity signals of less than a few micrometers of the heart wall that are superimposed on the motion of the heart wall due to the heart beat. There are several remarkable pulsatile waves during one cardiac cycle in the resultant velocity signals, some of them being commonly obtained for both healthy subjects and patients. These pulsatile waves cannot be recognized in standard echocardiography M-mode images. In this paper, by focusing on one pulsatile wave that occurs around the end-systole, the physiological meaning of these is considered based on various in-vivo experiments. The pulsatile wave measured by this novel ultrasonic method will offer potential for a quantitative assessment of myocardial viability. © 2000 Elsevier Science B.V. All rights reserved.

**Keywords:** Cardiac cycle; Isovolumetric relaxation period; Myocardial viability; Phased tracking method; Pulsatile wave

## 1. Introduction

Though M-mode echocardiography offers an advantage in critically looking at the motion pattern of the left ventricle (LV), its spatial resolution along the ultrasonic beam is limited to a few wavelengths, namely, only up to 1 mm for ultrasound of 3 MHz because an M-mode image is displayed based on the amplitude of the reflected ultrasound. However, numerous elaborate techniques have been proposed for non-invasive measurement of the velocity of the blood flow in the heart or the arteries based on the Doppler effect [1]. Moreover, several methods, including the phase-locked-loop (PLL) techniques, have been proposed to measure rough changes in the diameter of the arterial walls by tracking arterial wall displacement in real time [2,3].

For the accurate detection of velocity signals, that is, the instantaneous movement on or in the heart wall, we have developed the phased tracking method [4], which is briefly described in Section 2. This method has been validated by experiments using a water tank and has

been applied to in-vivo detection of small velocity signals, with sufficient reproducibility, on the wall of the human heart [4]. The detected velocity signals show rapid motion including high-frequency components with small amplitudes, which are difficult to recognize by M-mode echocardiography.

Moreover, the method has been applied to multiple points preset along an ultrasonic beam in the LV wall so that the instantaneous object positions,  $\{x_i(t)\}$ , and the velocity signals,  $\{v(x_i; t)\}$ , can be obtained for these multiple points,  $\{i\}$ , in the LV wall [5]. The wall changes position and thickness with time. By making the location of the RV side of the interventricular septum (IVS) the reference point, the thickness change during myocardial contraction/relaxation can be detected. Then, their spatial distribution is obtained and is superimposed on the M-mode image using color coding.

A spectrum analysis was first applied to the resultant non-invasively detected signals to identify the frequency band for the components from 25 to 90 Hz due to the myocardial thickening and thinning. Such an analysis shows the novel possibility of diagnosis of the regional myocardium [4,5].

The top three panels of Fig. 1 show the typical

\* Corresponding author. Fax: +81-22-263-9444.

E-mail address: hkanai@ecei.tohoku.ac.jp (H. Kanai)

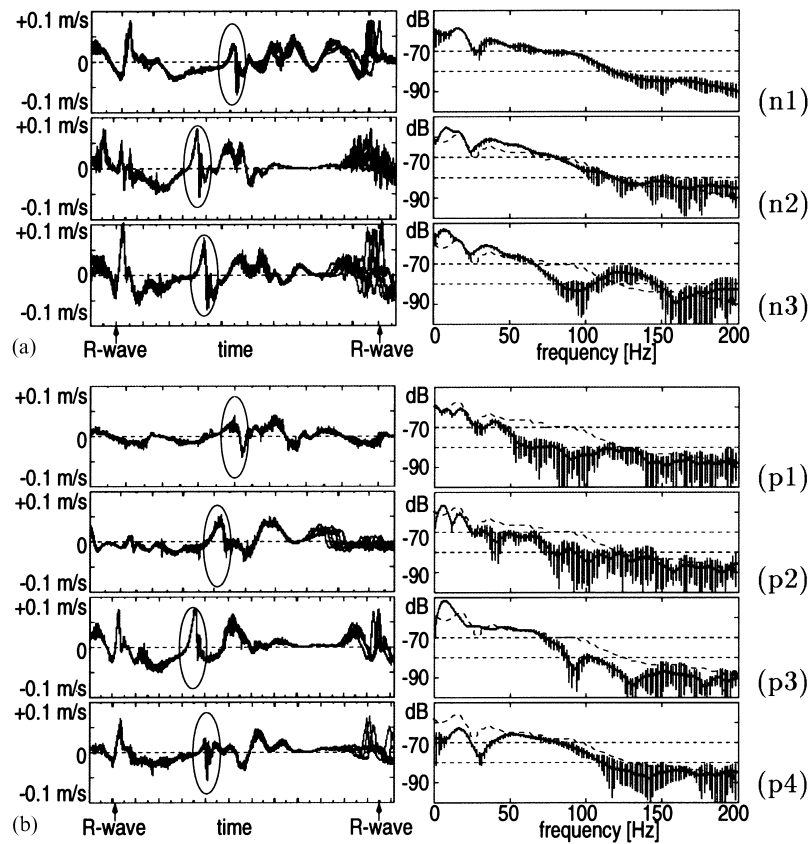


Fig. 1. In-vivo experimental results firstly obtained by the novel method [4]. Left: waveforms of the vibration signal on the LV side of the IVS (several heartbeats overlaid). The pulsatile wave interesting in this study is surrounded by an oval for each subject. Right: their average power spectra. Upper three rows of plots: for three healthy young male volunteers. (n1) Healthy 22 year old male volunteer. (n2) Healthy 26 year old male volunteer. (n3) Healthy 22 year old male volunteer. For each subject, the reproducibility is quantitatively confirmed up to 100 Hz. The waveforms and power spectra of these volunteers are similar. Bottom four: for three patients, with acute lymphoblastic leukemia, who have been treated with antineoplastic drugs (mitoxantrone). (p1) A 32 year old male patient. The measurement was performed 2 months before his death. (p2) Same patient as (p1). The measurement was performed 3 months before the measurement of (p1). (p3) 23 year old male patient. (p4) 25 year old female patient. The dotted lines overlaid show the power spectrum of the subject (n1).

waveforms of the vibration signals and their average power spectra, measured by the phased tracking method on the LV side of the IVS of three healthy young male volunteers [4]. The waveforms of several heartbeats are overlaid on each plot. For each subject, the reproducibility is quantitatively confirmed up to 100 Hz. The bottom four panels of Fig. 1 show the waveforms for four patients with cardiomyopathy induced by adriamycin injection. For all seven subjects, there are pulsatile waves around the isovolumetric relaxation period, indicated by the ovals in Fig. 1. The waveforms of the pulsatile waves (marked by ovals) of the patients in Fig. 1(p1), (p2), and (p4) are somewhat different from those for the healthy volunteers in Fig. 1(n1)–(n3).

In the right portion of Fig. 1, the average power spectra of the vibration signals around the pulsatile waves for several heartbeats are shown by solid curves. The power of the vibration in the patients, except for patient (p3), is decreased by at least several decibels as compared with that of the healthy subjects, which shows

the possibility to diagnose the ventricular dysfunction.

It is well known that the second heart sound (II) is radiated mainly by the closure of the aortic (Ao) valve. However, the cause and mechanism of the pulsatile waves in Fig. 1 remain unclear.

In this study, therefore, the novel method that we developed is modified and applied to the IVS and the posterior wall of the LV of healthy young volunteers. By comparing the timing of the pulsatile waves with the timing of the Ao valve closure, new findings that characterize the pulsatile waves are obtained. Finally, the timing of the pulsatile wave on the IVS is compared with the waveform of the LV inner pressure, which is simultaneously measured in an in-vivo experiment.

## 2. Principles of phased tracking method

Radio frequency pulses with an angular frequency of  $\omega_0 = 2\pi f_0$  are transmitted with a repetition period of

$\Delta T$  from an ultrasonic transducer. The ultrasonic pulse reflected by the object ( $i$ ) is received by the same ultrasonic transducer. The output signal is amplified and quadrature-demodulated. The resultant in-phase and quadrature signals for each transmitted pulse are simultaneously A/D-converted at a sampling frequency of  $1/T_s$ , and these two signals are combined into a complex signal,  $y(x; t)$ , where  $x(t)$  and its simple expression  $x$  denote the depth from the ultrasonic transducer. We assume that point  $i$  has only a velocity component that is parallel to the direction of the beam if the direction and position of the ultrasonic beam are appropriately selected so as to be perpendicular to the wall during the cardiac cycle. The instantaneous depth,  $x_i(t)$ , of the object ( $i$ ) from the ultrasonic transducer is given by the product of the acoustic propagation velocity,  $c_0$ , and the instantaneous period,  $\tau_i(t)$ , required for one-way transmission from the ultrasonic transducer to the object ( $i$ ). The phase  $\theta(x_i; t)$  of the signal  $y(x_i; t)$  is given by the angular frequency,  $\omega_0$ , multiplied by twice the delay time,  $\tau_i(t)$ . Thus, the phase difference,  $\Delta\theta(x_i; t)$ , between the analytic signals  $y(x_i; t)$  and  $y(x_i; t + \Delta T)$  of the successively received signals in the interval  $\Delta T$  is given by

$$\begin{aligned} \Delta\theta(x_i; t) &= \theta(x_i; t + \Delta T) - \theta(x_i; t) \\ &= 2\omega_0 \{ \tau_i(t + \Delta T) - \tau_i(t) \} = \frac{2\omega_0}{c_0} \Delta d_i(t), \end{aligned} \quad (1)$$

where  $\Delta d_i(t) = x_i(t + \Delta T) - x_i(t)$  is the instantaneous movement of the object ( $i$ ) in the period  $\Delta T$  after a time  $t$ . Then,  $\Delta d_i(t)$  is given from the measured data by:

$$\overline{\Delta d_i}(t) = c_0 \frac{\Delta\theta(x_i; t)}{2\omega_0} \quad (\text{m}). \quad (2)$$

Since it is essential to accurately determine the phase change  $\Delta\theta(x_i; t)$  of Eq. (2) during the period  $\Delta T$ , a complex correlation is employed in the determination procedure of the instantaneous movement of the object position,  $x_i(t)$  [4]. By dividing the estimate of the movement,  $\overline{\Delta d_i}(t)$ , by  $\Delta T$ , the velocity signal is given as follows:

$$\overline{v_i}(t) = c_0 \frac{\overline{\Delta d_i}(t)}{\Delta T} \quad (\text{m/s}). \quad (3)$$

The velocity signal and the spectrum are effective in diagnosis of the regional myocardium [5].

The position  $x_i(t)$  of the object ( $i$ ) in the heart wall changes by more than 10 mm due to the heartbeat in one cardiac cycle. It is, therefore, essential to track the instantaneous object position,  $x_i(t)$ . For this purpose, by accumulating the estimate,  $\overline{\Delta d_i}(t)$ , of the instantaneous movement in Eq. (2), the next object position,

$$\begin{aligned} \overline{x_i}(t + \Delta T), \text{ is estimated by} \\ \overline{x_i}(t + \Delta T) = \overline{x_i}(t) + \overline{\Delta d_i}(t) \quad (\text{m}). \end{aligned} \quad (4)$$

Thus, the instantaneous movement,  $\overline{\Delta d_i}(t)$ , and the next object position,  $\overline{x_i}(t + \Delta T)$ , are simultaneously determined and are obtained as waveforms.

When the time interval,  $\Delta T$ , of the transmission of the r.f. pulses is about 200  $\mu\text{s}$ , the maximum value of the instantaneous movement,  $\Delta d(t)$ , of an object in the heart wall is about 20  $\mu\text{m}$  during the time interval  $\Delta T$ . These values are much less than the wavelength of about 500  $\mu\text{m}$  at 3 MHz. Since the quadrature-demodulated signals are A/D-converted at a sampling interval,  $T_s$ , of 1  $\mu\text{s}$  in this paper, the spatial resolution  $\Delta x_s = T_s \times c_0 / 2 = 750 \mu\text{m}$  in the direction of depth. However, the resultant estimate  $\overline{x_i}(t)$  of the next object position of Eq. (4) in the above procedure is represented not by a discrete value, which depends on the sampling interval,  $T_s$ , but by the continuous value which is determined from the phase difference,  $\overline{\Delta\theta_i}(x_i; t)$ . Thus, accurate tracking of the object is realized by this method, and a small instantaneous movement in the order of several microns is determined.

To accurately consider the difference between the radiation timing of the pulsatile wave and the closure timing of the Ao valve, the ultrasonic pulse is alternately transmitted in two different directions, A and B, using a phased array transducer; one direction includes the Ao valve, and the other includes the IVS or the LV free wall. The velocity signals,  $v_{A_i}(t)$  and  $v_{B_j}(t)$ , are simultaneously measured at points  $i$  and  $j$ , each of which is in the direction of A and B of the ultrasonic beams, respectively.

### 3. In-vivo experiments along the longitudinal axis

First, the proposed method is applied to the detection of velocity signals on the wall of the aorta just anterior to the Ao valve, the IVS and the free wall of the LV of a healthy 24 year old male volunteer. The bottom right portion of Fig. 2 shows the cross-sectional B-mode images of these walls along the longitudinal axis, which were obtained by standard ultrasonic diagnostic equipment. The directions of the ultrasonic beams are set, as shown by the white lines A and B. Five points  $\{A_1, A_2, B_1, B_2, B_3\}$  are set along these ultrasonic beams.

Since the results obtained by the proposed method depend on the angle between the direction of the velocity vector and the ultrasonic beam, the direction of the ultrasonic beam passing through these walls is selected so that the beam is almost perpendicular to each wall during the A/D conversion of several cardiac cycles. During the acquisition period, respiration is suspended.

Fig. 2(b) and (c) show the ECG and the phonocardiogram (PCG), respectively. Before applying the method

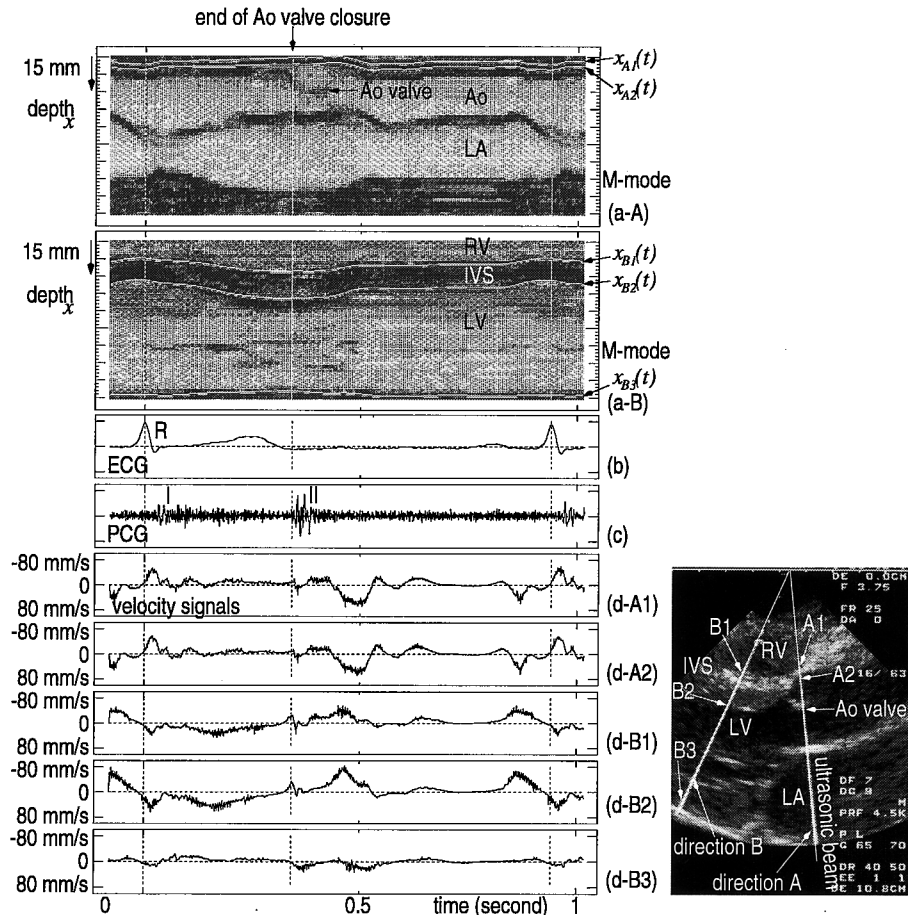


Fig. 2. In-vivo experimental results on (A) the Ao wall and (B) the IVS and LV posterior wall of a healthy 24 year old male volunteer. Right: cross-sectional B-mode image with the longitudinal axis showing the directions, A and B, of the ultrasonic beams and five object points,  $A_1$ ,  $A_2$ ,  $B_1$ ,  $B_2$ , and  $B_3$ , set along the beams. (a) Tracking results  $\{x_{A_i}(t)\}$  and  $\{x_{B_j}(t)\}$  for the five points  $\{A_i\}$  and  $\{B_j\}$  are shown by white lines on the M-mode images of the respective directions, A and B. From (a-A), the timing of the Ao valve closure is determined and is shown by the vertical dashed lines. (b) ECG. (c) PCG. (d) Velocity signals  $\{v_{A_i}(t)\}$  and  $\{v_{B_j}(t)\}$  of the points  $\{A_i\}$  and  $\{B_j\}$ .

described in Section 2, by referring to the M-mode image, which was reconstructed from the magnitude of the digitized signal of the analytic signals, the positions of the multiple points along the ultrasonic beam are manually preset in the workstation. The tracking results  $\{\overline{x_{A_i}(t)}\}$  or  $\{\overline{x_{B_j}(t)}\}$ , estimated by Eq. (4) of the points  $\{A_i\}$  or  $\{B_j\}$ , are superimposed on the M-mode image by white lines, as shown in Fig. 2(a-A) and (a-B). From Fig. 2(a-A), the timing of the Ao valve closure is determined and is shown by the vertical dashed lines.

Fig. 2(d-A1), (d-A2), (d-B1) (d-B2), and (d-B3) show the velocity signals  $\{\overline{v_{A_i}(t)}\}$  or  $\{\overline{v_{B_j}(t)}\}$  on the tracked points  $\{\overline{x_{A_i}(t)}\}$  or  $\{\overline{x_{B_j}(t)}\}$ . In order to ease interpretation, the vertical axis of these figures is inverted so that the negative value of the velocity, which is shown above the baseline, corresponds to the situation in which the object moves in the direction of the ultrasonic transducer on the chest wall. The resultant velocity signals are reproducible for the heartbeat periods.

#### 4. In-vivo experiments from the apex of the heart

Next, the proposed method is applied to the detection of velocity signals on the IVS and the LV posterior wall of a healthy 26 year old female volunteer, as shown in Figs. 3 and 4, respectively. The right panel of Fig. 3 and that of Fig. 4 show the cross-sectional B-mode images of these walls from the apical view. The directions of the ultrasonic beams are set as shown by the white lines A and B. Six points from  $\{B_1\}$  to  $\{B_6\}$  in the IVS in Fig. 3 and four points from  $\{B_1\}$  to  $\{B_4\}$  in the LV posterior wall in Fig. 4 are set along the ultrasonic beam B.

The tracking results  $\{\overline{x_{B_j}(t)}\}$ , estimated by Eq. (4) of the points  $\{B_j\}$ , are superimposed on the M-mode image by white lines, as shown in Figs. 3(a) and 4(a). From the M-mode image for the direction A of the ultrasonic beam, the timing of the Ao valve closure is determined and is shown by the vertical dashed lines. Figs. 3(d) and

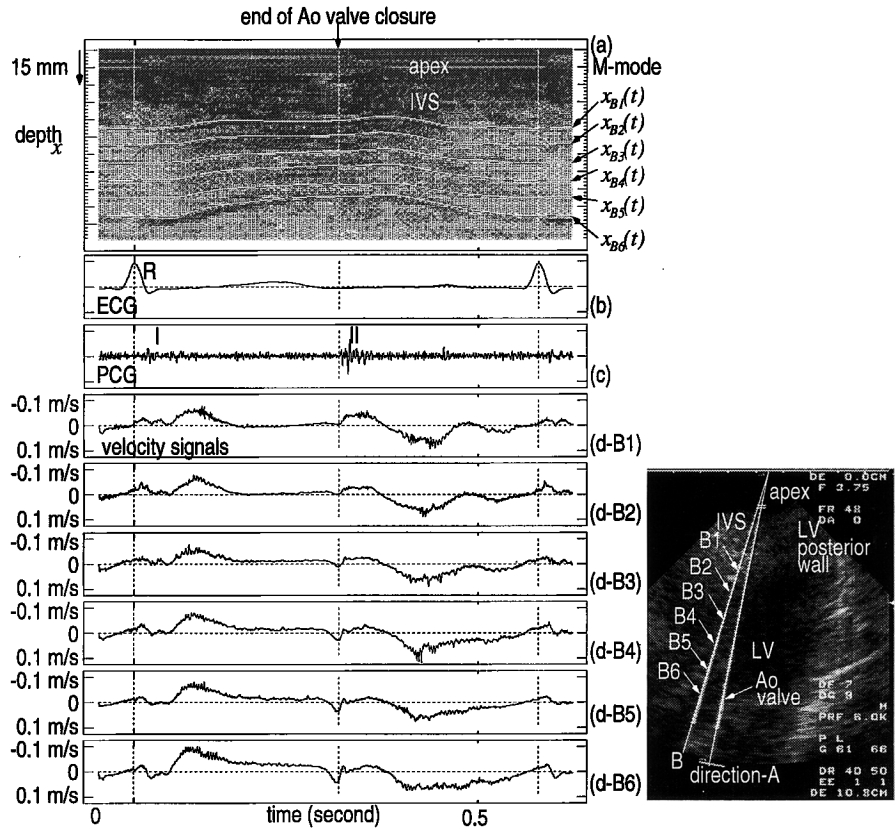


Fig. 3. In-vivo experimental results on (B) the IVS of a healthy 26 year old female volunteer. Right: cross-sectional B-mode image with the apical view showing the directions, A and B, of the ultrasonic beams and six object points from B<sub>1</sub> to B<sub>6</sub> set in the IVS along the beam B. (a) Tracking results  $\{x_{B_j}(t)\}$  for the six points  $\{B_j\}$  are shown by white lines on the M-mode image. From the M-mode image of the direction A, the timing of the Ao valve closure is determined and is shown by the vertical dashed lines. (b) ECG. (c) PCG. (d) Velocity signals  $\{\overline{v_{B_j}}(t)\}$  of the points  $\{B_j\}$ .

4(d) show the estimates of the velocity signals  $\{\overline{v_{B_j}}(t)\}$  on the tracked points  $\{\overline{x_{B_j}}(t)\}$ .

### 5. Simultaneous measurement of pulsatile wave and LV inner pressure

Finally, we applied the developed method to the IVS of a 57 year old male patient with dilated cardiomyopathy (DCM). The M-mode image, the ECG, and the waveforms of the velocity signals of the IVS are shown in Fig. 5(a), (b), and (d), respectively. In these measurements, the inner pressure of the LV is simultaneously measured by catheterization. The pressure is shown in Fig. 5(c). The two vertical dashed lines  $\tau_1$  and  $\tau_2$  show the starting time of the pulsatile wave on the LV side of the IVS and the location of the peak, respectively.

### 6. In-vivo experimental results and discussion

From the results in Fig. 2–5, which were all obtained by the newly developed method, there are several new findings, which cannot be recognized in the M-mode image of standard echocardiography:

1. As shown by Fig. 2(d-B1) and (d-B2), there are clear pulsatile waves on the IVS, each of which starts about 20 ms prior to the closure of the Ao valve. The velocity components in these figures are detected in the direction of the ultrasonic beam B, which is almost perpendicular to the IVS.
2. Similar results are obtained for a different subject, as shown in Fig. 3(d), where the velocity components are detected in the direction from the apex to the base of the heart.
3. Specifically just before the Ao valve closure, the velocity of the IVS is about 20 mm/s toward the right ventricle (RV) and toward the base of the heart.
4. Thus, from the timing described above, the pulsatile waves are not caused by the closure of the Ao valve. However, in the latter half of the pulsatile waves on the IVS, there are rapidly changing components, which may correspond to the second heart sound caused by the closure of the Ao valve.
5. As shown by Fig. 2(d-B3), the LV posterior wall has a pulsatile wave slightly slower than those on the IVS and it starts upon commencement of Ao valve closure. Surprisingly, similar waveforms are obtained for the different subjects in the apical view, as shown in Fig. 4(d-B3).

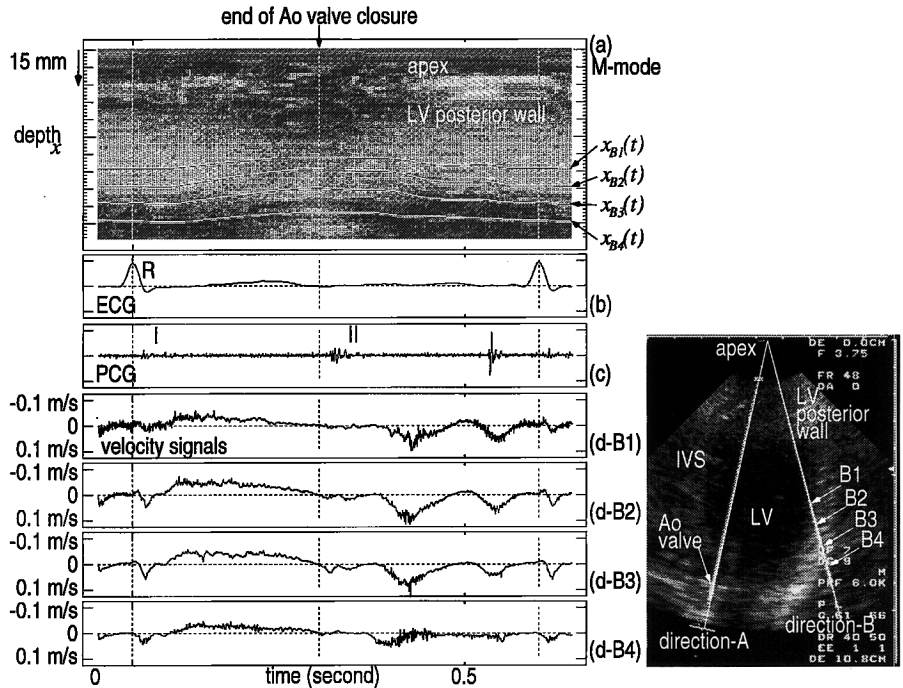


Fig. 4. In-vivo experimental results on (B) the IVS of the same volunteer as Fig. 3. Right: cross-sectional B-mode image with the apical view showing the directions, A and B, of the ultrasonic beams and four object points from B<sub>1</sub> to B<sub>4</sub> set in the LV posterior wall along the beam B. (a) Tracking results  $\{x_{B_j}(t)\}$  for the four points  $\{B_j\}$  are shown by white lines on the M-mode image. From the M-mode image of the direction A, the timing of the Ao valve closure is determined and is shown by the vertical dashed lines. (b) ECG. (c) PCG. (d) Velocity signals  $\{v_{B_j}(t)\}$  of the points  $\{B_j\}$ .

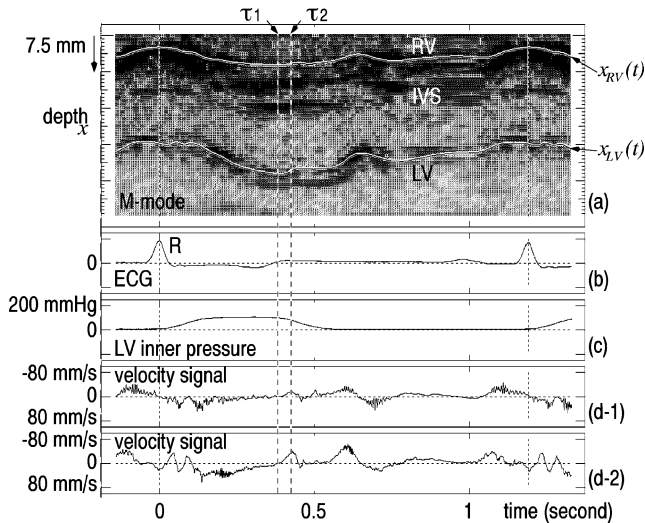


Fig. 5. In-vivo experimental results from the IVS of a 57 year old male patient with dilated cardiomyopathy (DCM). (a) M-mode image and the tracking results  $x_{RV}(t)$  and  $x_{LV}(t)$ . (b) ECG. (c) Inner pressure of the LV. (d-1) Velocity signals  $\{v(x_{RV}; t)\}$  of the RV side of the IVS. (d-2) Velocity signals  $\{v(x_{LV}; t)\}$  of the LV side of the IVS. The two vertical dashed lines A and B show the starting time of the pulsatile wave on the LV side of the IVS and the temporal location of the peak of this wave, respectively.

6. The direction of the pulsatile waves on the LV posterior wall in Fig. 3(d-B3) is opposite that on the IVS in Fig. 2(d-B1) and (d-B2). Thus, all the pulsatile

waves on the IVS in Fig. 2(d-B1) and (d-B2), and 3(d) and the LV posterior wall in Figs. 3(d-B3) and 4(d-B3) have velocity components, indicating that the lumen of the LV expands upon commencement of Ao valve closure.

7. By comparing the amplitudes of the pulsatile waves  $\{v_{B_j}(t)\}$  in Fig. 3(d-B1) with those in Fig. 3(d-B6), it can be seen that there are spatial distributions in their velocity values and that the IVS near the base has the highest velocity at the timing. Similar phenomena are obtained for the LV posterior wall, as shown in Fig. 2(d).
8. The velocity signals at the wall of the orifice just behind the Ao valve are measured in Fig. 2(d-A1) and (d-A2). The waveforms of the pulsatile waves around the timing of the Ao valve closure are similar to those obtained on the IVS in Fig. 2(d-B1) and (d-B2). However, the former is somewhat slower than the latter, and there is some delay from the latter to the former. These phenomena also support the fact that the pulsatile waves on the IVS do not originate from the closure of the Ao valve.
9. As shown by the vertical dashed line,  $\tau_1$ , in Fig. 5(c) and (d-2), the onset of the pulsatile wave corresponds to the point when the decrease in the LV inner pressure starts at the end of the ejection period.
10. At the point in time corresponding to the dashed line,  $\tau_2$ , in Fig. 5, the pulsatile wave on the LV side

of the IVS has reached its maximal velocity, and at this point in time, the Ao valve has just closed, as shown in Fig. 2(d-B1) and (d-B2).

Therefore, it seems very likely that the detected pulsatile wave originates from the myocardial relaxation and that there is a close relationship between the pulsatile wave and decrease in the LV inner pressure, which will be a direct cause of the Ao valve closure.

## 7. Conclusions

The findings reported here show the timing difference between the closure of the Ao valve and the pulsatile waves on the IVS and the LV posterior wall, which were first able to be measured by the novel phased tracking method. From the in-vivo experimental results, the pulsatile waves on the IVS and on the LV posterior wall are caused just before and just after the closure of the Ao valve, respectively. Thus, the pulsatile wave on the IVS does not originate from the closure of the Ao valve but originates in the myocardial contraction–relaxation sequence. The waveforms and their power spectra in Fig. 2 can be a significant clue for the diagnosis of the myocardial viability. From the in-vivo experiments of this paper, the pulsatile wave on the IVS starts 20 ms before the onset of the closure of the aortic valve. In

the latter half of the pulsatile waves on the IVS, however, rapidly changing components are included and they may correspond to the second heart sound, which is caused by the closure of the Ao valve. Thus, further investigations, including experiments using animals, are needed to confirm the the origin of these results.

## Acknowledgements

This work was supported in part by a Grant-in-Aid for Scientific Research (No. 10555134, 10650400) from the Ministry of Education, Science and Culture of Japan, and in part by the Sound Technology Promotion Foundation.

## References

- [1] C. Kasai, K. Namekawa, A. Koyama, R. Omoto, *IEEE Trans. Sonic Ultrason.* SU 32 (1985) 458.
- [2] A.P.G. Hoeks, C.J. Ruissen, P. Hick, R.S. Reneman, *Ultrasound Med. Biol.* 11 (1985) 51.
- [3] D.E. Hokanson, D.J. Monzersky, S.D. Sumner, D.E. Strandness Jr., *J. Appl. Physiol.* 32 (1972) 728.
- [4] H. Kanai, M. Sato, Y. Koiwa, N. Chubachi, *IEEE Trans. Ultrason. Ferroelectr. Freq. Cont.* 43 (1996) 791.
- [5] H. Kanai, H. Hasegawa, N. Chubachi, Y. Koiwa, *IEEE Trans. Ultrason. Ferroelectr. Freq. Cont.* 44 (1997) 752.